ResearchGate

See discussions, stats, and author profiles for this publication at: https://www.researchgate.net/publication/231637482

Investigation of the Photoionization Mechanism of Small Aromatic Homoclusters

ARTICLE *in* THE JOURNAL OF PHYSICAL CHEMISTRY A · APRIL 2004

Impact Factor: 2.69 · DOI: 10.1021/jp036761g

CITATIONS
3

READS
15

3 AUTHORS, INCLUDING:

Benjamin Bouvier
Institute for the Biology and Chemistry of Pro…
17 PUBLICATIONS **379** CITATIONS
SEE PROFILE

Michel Mons
Atomic Energy and Alternative Energies Com…
130 PUBLICATIONS **3,221** CITATIONS
SEE PROFILE

Available from: Benjamin Bouvier
Retrieved on: 23 January 2016

Investigation of the Photoionization Mechanism of Small Aromatic Homoclusters

Benjamin Bouvier,* Philippe Millié, and Michel Mons

Laboratoire Francis Perrin, URA 2453, DSM/DRECAM/SPAM, CEA Saclay, Bât. 522, 91191 Gif-sur-Yvette, France

Received: September 16, 2003; In Final Form: February 24, 2004

This work proposes to simulate the direct photoionization process of small aromatic clusters of benzene, naphthalene, and anthracene, using the combination of a tailored model potential and a valence bond Hamiltonian. Classical molecular dynamics simulations are carried out on the potential energy surface of the neutral cluster, at energies meant to transcribe quantum mechanical effects such as intermolecular vibrational zero-point energy and the classically forbidden area of the vibrational ground-state wave function. The statistics of the ionization potential values obtained by vertical ionization of neutral configurations originating from these simulations yield valuable information on the respective topologies of the neutral and ionic potential energy surfaces. Comparison of calculated values with experimental one-photon and two-photon ionization potential determinations and ion current curves is also performed.

1. Introduction

Molecular clusters of aromatic compounds have been of interest to the theoretical and the experimental physical chemistry communities for a long while. They provide insight into the mechanisms of π interactions, which are as ubiquitous as they are complex. Aromatic and heteroaromatic moieties are present in many compound systems such as biopolymers and liquid crystals, and may often be held responsible for important properties of such systems. Molecular ions of aromatic assemblies also have attracted great attention. The correct description of their electronic states, albeit more complex than that of the corresponding neutral clusters, is necessary to study important phenomena such as charge transfer or charge transport in large systems. These phenomena are largely based on the interplay between the ionic and neutral varieties of local aromatic moieties, as well as their interactions as part of a larger system (DNA, for example[1−3]).

It is widespread knowledge that aromatic clusters, whether neutral or charged, are complicated to characterize from the theoretical point of view.[4] Neutral clusters are most conveniently described using model potentials,[5−9] since ab initio calculations on such systems require high—and costly—levels of theory;[10] these calculations may however be mandatory if the model potential is to be correctly calibrated. Ionic clusters raise a different issue altogether. Their properties differ tremendously from those of their neutral counterparts, mainly because of charge resonance phenomena which are theoretically complicated to account for.

A previous paper[9] addresses these questions in much more detail. It combines a tailored model potential and an effective Hamiltonian approach to provide a correct description of both charged and neutral species, as well as charge resonance phenomena bridging the gap between both, for a set of aromatic homoclusters of benzene, naphthalene, and anthracene. This methodology was applied to the extensive study of the topology of the potential energy surfaces (PESs) of both neutral and ionized clusters, yielding global and local minima and their relative binding energies. Comparison to both experimental data and high-level ab initio calculations, whenever available, confirmed the validity of this approach. Using data gathered from PES topologies, theoretical "vertical" and "adiabatic" ionization potentials (IPs) were determined. However, the experimentally measured ionization potential is more likely between these two values.

The present study focuses more acutely on this last issue. The first photoionization potentials of small aromatic homoclusters (benzene, naphthalene, and anthracene, with coordination numbers up to 4) were previously inferred from global 0 K PES explorations. They are to be tackled, in the present study, from the standpoint of classical molecular dynamics simulations on the PES associated with the electronic ground state of the neutral cluster, using the model potential whose reliability already has been demonstrated. The energies at which these simulations are led are chosen to model quantum effects such as the exploration of the classically forbidden part of the vibrational ground-state wave function of the neutral cluster. Configurations originating from these simulations are assumed to be vertically ionized, and the IP statistics thus obtained are described and analyzed. This model is compatible with a direct photoionization mechanism, and does not take vibrational autoionization into account. The validity of this assumption, which rests on theoretical considerations (see section 3.4), will be examined in light of comparison with experiment.[11−18]

2. Methodology

2.1. Model Potential. The intermolecular model potential used in this work has been thoroughly described in the last installment of this work,[9] and shall only be succinctly outlined in the present paper. On the basis of second-order perturbation theory, it contains individual terms corresponding to electrostatic, dipole polarization, dispersion, and repulsion contributions to the intermolecular interaction energy. The electrostatic term originates from interactions between distributed multipoles (up to the quadrupole) fitted from a one-particle density matrix ab initio calculation. The polarization energy is inferred from a

* To whom correspondence should be addressed. Phone: +33-1-6908-3788. Fax: +33-1-6908-8707. E-mail: bouvier@pandora.saclay.cea.fr.

10.1021/jp036761g CCC: $27.50 © 2004 American Chemical Society
Published on Web 04/17/2004

self-consistent approach using anisotropic site polarizabilities explicitly designed for aromatics. The dispersion and repulsion terms are two-body terms based on atom-specific parameters. A neutral aromatic moiety and its charged counterpart share the same dispersion and repulsion interactions but have distinct electrostatic and polarization parameters. Intramolecular rearrangement upon ionization was neglected, the neutral and the ionic forms of each monomer sharing the same geometry. This can be considered a good approximation for aromatics, despite a limited Jahn−Teller effect in the benzene cation.[19]

2.2. Effective Hamiltonian Framework. Charge-transfer interactions in aromatic homoclusters are described via a valence bond treatment, using an effective Hamiltonian written out in the basis of all possible cluster configurations where the charge is localized on a given monomer, and whose energies are determined using the aforesaid model potential. Coupling elements between these basis wave functions are considered proportional to overlap integrals between the molecular orbitals of the charged monomers that are implicated in the electron transfer, on each of the two valence bond forms. The proportionality factor is a monomer-dependent environment-independent parameter which is computed from ab initio selected configuration interaction calculations on the corresponding dimer cluster. Diagonalization of the effective Hamiltonian yields ground- and excited-state wave functions for the supersystem. A single ionization potential per monomer is explicitly considered, higher IPs being neglected. This is a reasonable approximation for the description of neutral and charged clusters in their electronic ground state. Details on the parametrization of the potential, including reference ab initio calculations, may be found in ref 9.

2.3. Quantum Description of the Photoionization Process. Neutral and ionized clusters of aromatic molecules such as benzene, naphthalene, and anthracene have been shown to possess very different structures. Therefore, adiabatic photoionization to the vibrational ground state of the ion is forbidden by the Franck−Condon principle. Ionization may only lead to high-lying excited intermolecular vibrational states of the ion, which enable the ion complex to explore conformations similar to those of the neutral ground state. An experimental signature of such a peculiarity is the slow rise of the photoionization current at the onset, found, for example, for the $(benzene)_2$ cluster.[11,12,14,18]

In molecular jet experiments, neutral aromatic clusters are mainly formed in their vibrational ground state, at temperatures typically lower than 10 K. This suggests that the threshold photoionization process of such clusters should be addressed in terms of the spatial extent of the neutral vibrational ground-state wave function. Due to the differences in the oscillating behavior of this wave function and that of the high-lying vibrationally excited states of the ion cluster, the only nonvanishing contribution to the Franck−Condon overlap originates from the classically forbidden parts of the neutral wave functions (Figure 1). This work attempts to emulate this quantum mechanical behavior with classical molecular dynamics as a tool.[20,21]

2.4. Molecular Dynamics Calculations. Classical molecular dynamics was chosen as a means to sample the classically forbidden area of the vibrational ground state of the neutral cluster. It allows explicit consideration of all intermolecular degrees of freedom, which is particularly useful for cases where the relevant intermolecular coordinate q (Figure 1) is not an eigenmode of the system, but a combination of several eigenmodes. Rigid-body molecular dynamics calculations on neutral

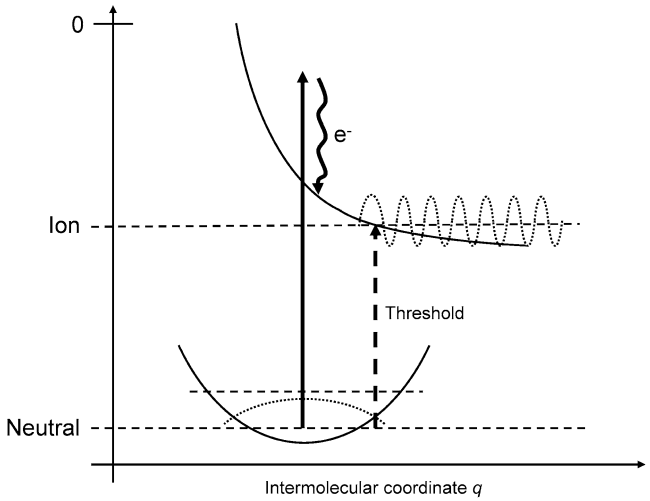

Figure 1. Schematic representation of the potential energy surfaces of the neutral and ionic clusters, in the regions relevant to the photoionization process. The vibrational wave functions for the neutral ground state and a highly excited ionic state are plotted along an arbitrary intermolecular coordinate q. The dashed arrow materializes the position of the threshold. The full arrow denotes a vertical transition from the neutral potential energy surface, the ejected electron (e^-, wavy arrow) taking away the excess energy.

aromatic clusters are carried out on the PES associated with the model potential, in the microcanonical (N, V, E) ensemble. As a consequence, intramolecular vibrations of the monomers were neglected. The configurations that we wish to sample are those belonging to the classically forbidden part of the vibrational ground-state wave function. They can be accessed through a microcanonical molecular dynamics calculation if the total energy of the system (potential plus kinetic) is higher than the value of the zero-point energy (ZPE). As an example, the theoretical ZPE for the neutral benzene dimer was found to be 130 K.[22]

The use of quaternions to describe molecular rotation bypasses gimbal lock issues. Forces are computed using analytical derivatives of the potential. Integration of translational movements resorts to the velocity Verlet algorithm, whereas the midstep implicit leapfrog algorithm due to Svanberg[23] is employed where rotational motion is concerned. Time steps of 2 fs were found consistent with a good energy conservation (fluctuations under 0.1%) for all systems under study.

2.5. Sampling of the Potential Energy Surfaces. Molecular dynamics calculations were performed at two different energies. Denoting the well-bottom energy of the neutral global minimum of the cluster as E_0, these energies were chosen to be $E_0 + 100$ K and $E_0 + 300$ K. The first simulation should give a reasonable description of the neutral cluster in its vibrational ground state (including the ZPE). The second one aims at simulating quantum effects, by giving access to configurations that are part of the classically forbidden region of the vibrational ground-state wave function.

The value of the ZPE is expected to vary depending on the cluster under study, so that using a single value (100 K) in all cases is an approximation. However, since this value is expected to increase with the aggregation number and to decrease in the series benzene−naphthalene−anthracene, employing a mean value has been deemed a good choice to compensate for the lack of adequate theoretical results. The choice of $E_0 + 300$ K to simulate quantum effects appeared as the best compromise between allowing the system to explore higher energy regions on its potential energy surface and preventing monomer

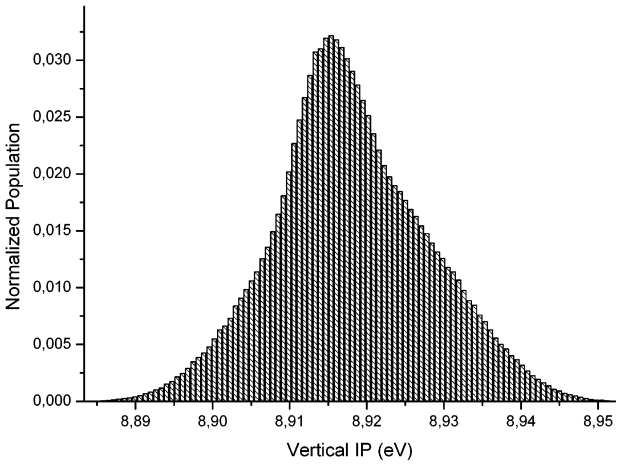

Figure 2. Histogram of IP values encountered during a 2 ns molecular dynamics simulation on the neutral $(benzene)_2$ cluster at energy E_0 + 100 K, where E_0 is the potential energy of the global minimum of the cluster.

evaporation, which, due to the weak binding energies of the monomers inside the neutral clusters, rapidly becomes an issue when the total energy is raised. The choice of this energy influences the theoretical determination of the ionization potentials of the clusters under study in a quantitative manner, but does not affect the qualitative ordering of these values for varying cluster sizes, or in the series benzene−naphthalene−anthracene, under discussion in this work.

Starting configurations for the molecular dynamics simulations were chosen to comply with the aforementioned energy criteria. Total simulation times were 2 ns in all cases.

2.6. Photoionization Probability Cross-Section. As already mentioned, the neutral molecular dynamics simulation aims at describing the cluster in its vibrational ground state, which is supposed to be the only one populated at typical molecular jet temperatures. Hence, the total energy of the neutral cluster was taken equal to the energy of the global minimum well bottom on the neutral potential energy surface (E_0), plus 100 K to account for the ZPE, and was supposed constant throughout the dynamics. The higher energy of E_0 + 300 K is designed to give access to configurations inside the classically forbidden region of the neutral ground-state wave function, which cannot be sampled by a classical simulation at E_0 + 100 K. These configurations, however, are part of the neutral vibrational ground state and share the same total energy of E_0 + 100 K, regardless of the total energy of the dynamics from which they were obtained. In the framework of the model, photoionization occurs via a vertical transition from classical configurations, the ejected electron taking away the excess energy; strictly speaking, this model is only valid at threshold. Resulting ion clusters may show varying energies, depending on the associated neutral cluster configuration from which the vertical ionization process occurred.

The geometry of the neutral cluster was extracted at each time step of the molecular dynamics simulation. At this geometry, the energy associated with the electronic ground-state wave function of the singly charged cluster was computed using the valence bond Hamiltonian model. Subtraction of the energy of the vibrational ground state of the neutral cluster from the energy of the ion cluster yielded an instant vertical ionization potential. These were compiled into a histogram, featuring the normalized count of configurations versus the values of the vertical IP. An example of such a graph, in the case of the benzene dimer at E_0 + 100 K, can be found in Figure 2.

TABLE 1: Intermolecular Binding Energy of the Vibrational Ground State of the Neutral Clusters under Study[a]

cluster	binding energy (eV)	cluster	binding energy (eV)	cluster	binding energy (eV)
$(benzene)_2$	−0.070	$(naphthalene)_2$	−0.127	$(anthracene)_2$	−0.182
$(benzene)_3$	−0.238	$(naphthalene)_3$	−0.424	$(anthracene)_3$	−0.596
$(benzene)_4$	−0.453	$(naphthalene)_4$	−0.665		

[a] The energy reference is that of n noninteracting monomer moieties (at infinite distances), where n denotes the aggregation number.

TABLE 2: Intermolecular Energy Ranges (as Minimum and Maximum) of the Ionic Clusters Encountered during the Simulation[a]

cluster	neutral energy	ion energy range (eV) min	ion energy range (eV) max	ion global min (eV)
$(benzene)_2$	E_0 + 100 K	−0.432	−0.363	−1.130
	E_0 + 300 K	−0.466	−0.225	
$(benzene)_3$	E_0 + 100 K	−0.770	−0.555	−1.522
	E_0 + 300 K	−0.820	−0.442	
$(benzene)_4$	E_0 + 100 K	−0.994	−0.753	−1.869
	E_0 + 300 K	−1.096	−0.522	
$(naphthalene)_2$	E_0 + 100 K	−0.482	−0.450	−0.856
	E_0 + 300 K	−0.488	−0.450	
$(naphthalene)_3$	E_0 + 100 K	−0.883	−0.721	−1.319
	E_0 + 300 K	−0.916	−0.575	
$(naphthalene)_4$	E_0 + 100 K	−1.338	−1.133	−1.765
	E_0 + 300 K	−1.343	−0.754	
$(anthracene)_2$	E_0 + 100 K	−0.553	−0.531	−0.758
	E_0 + 300 K	−0.562	−0.512	
$(anthracene)_3$	E_0 + 100 K	−0.995	−0.920	−1.333
	E_0 + 300 K	−1.002	−0.920	

[a] As a comparison, intermolecular binding energies of the global minimum of each ionic cluster potential energy surface are also given. The energy reference for a size n cluster ion is that of n − 1 neutral monomer moieties and one charged monomer moiety, at infinite distances.

The ion current associated with a given IP value was computed as the area of the histogram taken between the threshold and the IP, the total area of the histogram (taken between the minimum and the maximum thresholds) being normalized to unity.

3. Results and Discussion

3.1. Energy Ranges of Neutral and Ionic Clusters. Molecular dynamics simulations were run, at the two aforementioned energies, on neutral clusters of $(benzene)_2$ to $(benzene)_4$, $(naphthalene)_2$ to $(naphthalene)_4$, and $(anthracene)_2$ to $(anthracene)_3$, under the previously mentioned conditions. The energies of the vibrational ground states of the neutral clusters (E_0 + 100 K; see section 2.6) are given in Table 1. The energy ranges of the ionic clusters encountered during the molecular dynamics simulations are compiled in Table 2, along with the energy values of the global minimum on the corresponding ion potential energy surface.

As can be seen, in all cases the minimum and maximum values that bracket the ion energy range are much greater than the energy of the global minimum. This confirms the fundamental differences in the topologies of the potential energy surfaces of the ionic and neutral clusters, for which the location and nature of stationary points are very dissimilar. It is particularly remarkable in the clusters of benzene, where the difference may amount to more than 1 eV. This is consistent with the qualitative conclusions of our previous work,[9] and indicates that the true adiabatic ionization potential of these

TABLE 3: Characteristics of the IP Histograms for All Clusters under Study[a]

cluster	energy	maximum (eV)	thresholds (eV) lower	thresholds (eV) upper	width (eV)
$(benzene)_2$	$E_0 + 100$ K	8.92	8.88	8.95	0.07
	$E_0 + 300$ K	8.97	8.85	9.09	0.24
$(benzene)_3$	$E_0 + 100$ K	8.82	8.71	8.93	0.21
	$E_0 + 300$ K	8.87	8.66	9.04	0.38
$(benzene)_4$	$E_0 + 100$ K	8.82	8.70	8.95	0.24
	$E_0 + 300$ K	8.93	8.60	9.18	0.57
$(naphthalene)_2$	$E_0 + 100$ K	7.80	7.79	7.82	0.03
	$E_0 + 300$ K	7.80	7.78	7.82	0.04
$(naphthalene)_3$	$E_0 + 100$ K	7.75	7.68	7.84	0.16
	$E_0 + 300$ K	7.85	7.65	7.99	0.34
$(naphthalene)_4$	$E_0 + 100$ K	7.56	7.47	7.67	0.21
	$E_0 + 300$ K	7.81	7.46	8.05	0.59
$(anthracene)_2$	$E_0 + 100$ K	7.09	7.08	7.10	0.02
	$E_0 + 300$ K	7.09	7.07	7.12	0.05
$(anthracene)_3$	$E_0 + 100$ K	7.07	7.05	7.12	0.07
	$E_0 + 300$ K	7.07	7.04	7.12	0.08

[a] Maximum (IP value corresponding to the most frequently occurring neutral cluster structures), lower and upper thresholds (lowest and highest IP values observed during the simulation), and width (highest IP minus lowest IP).

clusters should not be experimentally available. Also noteworthy is the fact that, among the ion clusters encountered during this study, none were found to exhibit a dissociative character (i.e., the corresponding binding energy was always negative). This is interesting evidence that the experimentally observed dissociation upon ionization[15] is in fact due to the inter- and intramolecular vibrational energy deposited inside the ion cluster, which the present model does not pretend to transcribe.

A rise in total energy allows the system to explore a vaster area of the neutral potential energy surface and, following vertical ionization, of the ionic potential energy surface. This translates into a spread of the ionic cluster energy range. In some cases, the energy values bracketing this range show little to no variation upon an energy increase; this is characteristic of the fact that a local minimum (if the minimum bound does not vary) or maximum (if the maximum bound is constant) is being explored at both energies. Examples of this include the maximum brackets of the $(naphthalene)_2$ and $(anthracene)_3$ clusters. In the case of $(naphthalene)_2$, the local maximum was identified by local optimization as a first-order saddle point of T-shaped geometry, where the centers of mass of both monomers are separated by 4.99 Å (versus 5.15 Å for the neutral global minimum), and whose energy of $E_0 + 87$ K makes it accessible to both molecular dynamics simulations.

In most cases, however, both brackets do vary significantly: the difference amounts to ca. 0.4 eV for the upper limit of $(naphthalene)_4$, for example. This is evidence that the area of the ion potential energy surface under exploration is quite steep and fully justifies the need to take the classically forbidden part of the neutral wave function into account, as was simulated here by an increase of the total energy.

3.2. Ionization Potential Statistics. Histograms of vertical ionization potential values were generated, as previously explained, for all the clusters under study. An example of such a graph can be found in Figure 2. Table 3 presents the characteristic properties of these histograms.

Since the energy of the neutral cluster is supposed constant (Table 1), the upper and lower thresholds of the histograms are directly related to the corresponding brackets for the ionic cluster energies (Table 2). Hence, the trends discussed above still apply here: a rise in the total energy will globally be accompanied by an increase in the width of the histogram, but a given threshold may remain fixed if the area of the ion potential energy surface being explored features stationary points.

The maximum of the histogram is the center point of the most frequently occurring vertical IP subdivision, and represents the vertical ionization potential, which may be theoretically computed[9] or inferred from experimental ion current curves, as shall be seen hereafter. However, let us mention that, since the maximum value is generally far from the threshold, direct comparison of theoretical and experimental vertical ionization potentials should be subject to caution. The lower bracket of the histogram corresponds to the onset of the ion current curve and is the theoretical counterpoint to the experimentally determined threshold IP.

Cluster configurations resulting in IP values that are close to the maximum are those that play the most important role in the ionization process. Some clusters, for example, $(naphthalene)_3$ and $(naphthalene)_4$, feature an increase of the maximum when the total energy rises: the configurations responsible for ionization tend to occur at higher energies only. It is hence essential, for such clusters, to take into account all possible configurations, including those inside the classically forbidden region (which are accessed at $E_0 + 300$ K in the framework of our model). Moreover, these clusters are those for which the width of the histogram increases the most with the total energy. As previously mentioned, this is consistent with a very steep region on the ion potential energy surface, which probably corresponds to high-lying vibrationally excited states of the charged cluster; this stresses further the necessity to account for classically forbidden configurations on which the ionization process depends.

For other clusters such as $(anthracene)_2$ and $(anthracene)_3$, on the contrary, the maximum does not evolve with the total energy. In these cases, the configurations responsible for ionization are accessible at lower energies. The correct vertical IP value may be found regardless of the energy at which the neutral dynamics was performed; i.e., the configurations responsible for ionization are probably not located in the classically forbidden region of the neutral vibrational ground-state wave function. This can be interpreted by the proximity of a local minimum on the ion potential energy surface and the global minimum on the neutral potential energy surface: the vertical transition from the neutral vibrational ground state leads to a rather low-lying vibrationally excited state of the ion whose wave function overlaps that of the neutral vibrational ground state. This finding is in good agreement with our previous work,[9] where the large number of local minima on the potential energy surfaces of neutral and charged anthracene clusters had been mentioned.

3.3. Simulated Direct Photoionization Ion Current Curves. The aforementioned vertical IP histograms were integrated over their own width, to yield simulated ion current curves which will be compared to their experimental counterparts, whenever available, in the following paragraph. These curves may be found, for clusters of benzene, naphthalene, and anthracene, in Figures 3, 4, and 5, respectively. We once again stress the fact that, since our model neglects the intramolecular vibrationally excited states which, in reality, contribute to the experimental ion current curve, a rigorous comparison with our theoretical results is only feasible near the threshold. However, we have the feeling that interesting global trends may nevertheless be inferred from such a comparison.

The possibility of vibrational autoionization also needs to be considered, since a photoionization efficiency experiment cannot distinguish between ions due to this phenomenon and those

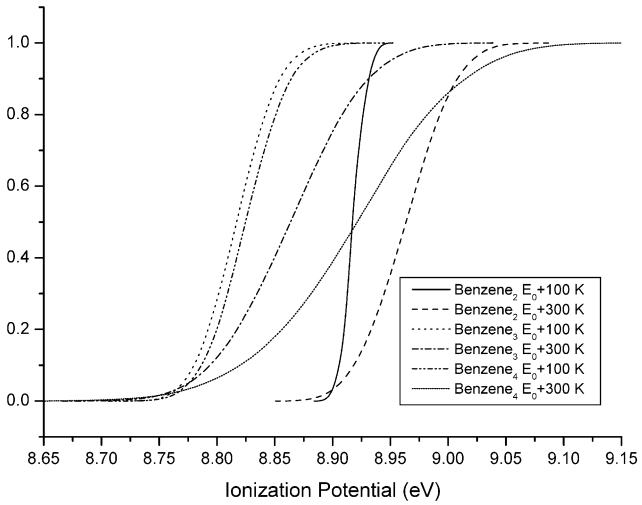

Figure 3. Simulated ion current curves for the clusters (benzene)$_n$, $2 \leq n \leq 4$, for two different neutral molecular dynamics energies (refer to the text).

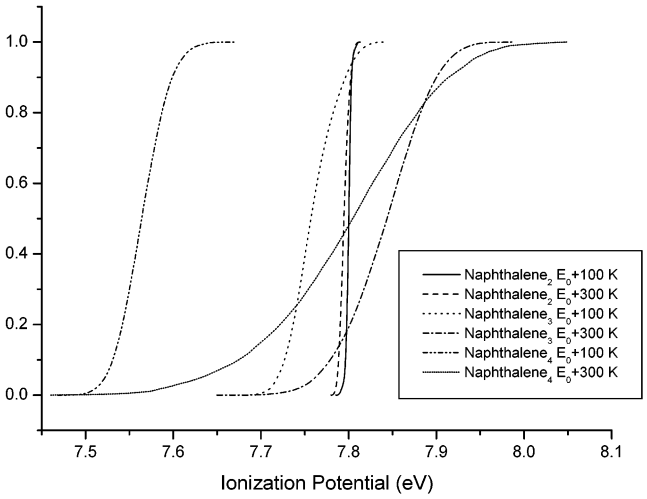

Figure 4. Simulated ion current curves for the clusters (naphthalene)$_n$, $2 \leq n \leq 4$, for two different neutral molecular dynamics energies (refer to the text).

resulting from direct photoionization. Evidence for internal conversion from the $3R_g$ Rydberg state of the benzene monomer, due to rotation−vibration−electron coupling between the Rydberg electron and the cationic core, has been experimentally provided.[24] A similar scheme could be suspected to occur in larger aromatic clusters featuring charged cores, such as the ones under study. However, as explained in section 3.4, this is in contradiction with available experimental data.

The onset of the ion current curves corresponds to the threshold ionization potentials appearing in Table 4. The steepness of the curves depends on two factors. First, the area of the neutral potential energy surface that is explored during the molecular dynamics simulations dictates the area visited on the ion potential energy surface following vertical ionization. Unless the ion potential energy surface in this zone is flat, a more widespread exploration of this surface tends to generate a wider range of ion energies, hence of vertical IP values, thereby resulting in widespread and gently rising ion current curves. On the other hand, the thoroughness of the exploration depends on the nature of the neutral potential energy surface: a steep surface will limit the exploration, even at high energies, and result in a more pronounced slope for the ion current. Second, a steep ion potential energy surface in the region under

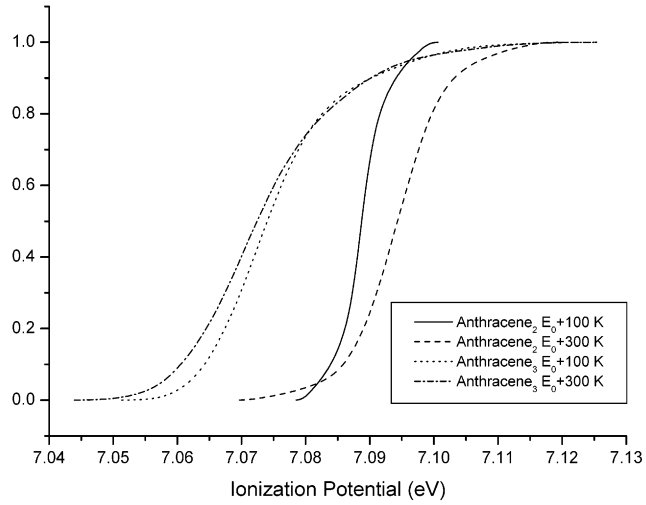

Figure 5. Simulated ion current curves for the clusters (anthracene)$_n$, $2 \leq n \leq 3$, for two different neutral molecular dynamics energies (refer to the text).

TABLE 4: Comparison of the Theoretical Threshold Values Calculated for the Clusters of Benzene and Naphthalene with Experimental Determinations from the Literature

cluster	energy	theoretical IP (eV)	exptl threshold (eV)
$(benzene)_2$	$E_0 + 100$ K	8.88	8.65 ± 0.01[12,15] (two-photon)
			$<8.865 \pm 0.004$[11,14] (two-photon)
	$E_0 + 300$ K	8.85	8.53 ± 0.03[16] (two-photon)
			8.69 ± 0.02[13,18] (one-photon)
$(benzene)_3$	$E_0 + 100$ K	8.71	8.58 ± 0.02[15]
	$E_0 + 300$ K	8.66	8.54 ± 0.03[16]
$(benzene)_4$	$E_0 + 100$ K	8.70	8.55 ± 0.02[15]
	$E_0 + 300$ K	8.60	
$(naphthalene)_2$	$E_0 + 100$ K	7.79	7.58 ± 0.04[25]
	$E_0 + 300$ K	7.78	
$(naphthalene)_3$	$E_0 + 100$ K	7.68	7.56 ± 0.03[25]
	$E_0 + 300$ K	7.65	
$(naphthalene)_4$	$E_0 + 100$ K	7.47	7.49 ± 0.03[25]
	$E_0 + 300$ K	7.46	

exploration will produce a wider range of IP values, hence a gentler slope for the ion current.

When the total energy of the neutral molecular dynamics simulation rises, the system is allowed to explore vaster regions on both the neutral and the ionic potential energy surfaces: ion current curves at $E_0 + 100$ K are generally steeper than their counterparts at $E_0 + 300$ K. This is especially true for clusters such as $(benzene)_2$ or $(naphthalene)_2$; in these cases, the structural difference between neutral and ionic clusters is such that configurations originating from the neutral molecular dynamics simulation correspond to high-lying ions located on steep areas far from any local minimum. Larger clusters are characterized by flatter potential energy surfaces featuring a large number of local minima; this results in more gentle slopes on the ion current curves, and a less marked dependence on the energy at which the neutral molecular dynamics calculation is carried out.

Finally, let us mention that the maximum value of the histogram (Table 3) corresponds to the inflection point on the ion current curve. This far from the threshold, a comparison between inflection points on theoretical and experimental ion current curves is probably not legitimate. However, as a tribute to our model, we note that the correspondence between the histogram maxima and the previously determined[9] 0 K vertical ionization potentials is quite good.

3.4. Comparison with Experiments. Here, we compare the lower threshold values of the IP histograms with the corre-

sponding experimentally determined "adiabatic" ionization potentials. These are most readily available for small benzene clusters;[11−18] a recently published work by Fujiwara and Lim[25] presents IP values for naphthalene aggregates; to our knowledge, such values are not known for clusters of anthracene. Table 4 reproduces the theoretically determined threshold IPs alongside their experimental counterparts, as taken from various published works. Additionally, the simulated ion current curves in Figures 3 and 4 are qualitatively compared to their experimental counterparts.

As previously mentioned, the possibility of vibrational autoionization via Rydberg states may be considered, since this process can a priori compete with direct photoionization. In the vicinity of the threshold, autoionization must proceed from the very dense manifold of intermolecular vibrational states. This density is expected to increase with the number of low-frequency intermolecular modes, i.e., with the number of monomers in the cluster. The efficiency of the autoionization process should thus be enhanced in larger aggregates, causing the corresponding experimentally determined IP to drop toward the adiabatic IP value. The cases of benzene and naphthalene, where the evolution of experimental IP values with the cluster size is known, do not feature such a quick decrease with the cluster size.[15,16,25] Moreover, the IP values are systematically quite far from the corresponding adiabatic limit, as computed in our previous study.[9] Hence, in the absence of any decisive experimental evidence for the occurrence of the vibrational autoionization phenomenon, we deem it to be negligible, at least near the threshold.

As can be seen, a consensus has yet to be reached as far as the experimental determination of the IP of $(benzene)_2$ is concerned. The only real point of concordance between experimental studies is the slow rise of the ion current with photon energy, which stems from the structural difference between the neutral and ionic cluster geometries already observed in our previous study.[9] Depending on the experimental technique (one-photon or two-photon), different Franck−Condon factors may be invoked to explain the ionization mechanism, resulting in different extrapolated IP values. The sensitivity of the techniques also has a determining influence on the extrapolated position of the threshold, especially in the case of two-color experiments that may suffer from a parasite one-color signal. This explains the rather important differences in values between refs 11 and 14 on one hand and refs 12 and 15 on the other. The latter experiments, being much more sensitive since optimized for the determination of the threshold, are more reliable than the former, which should rather be considered as an upper bound for the threshold (despite the reported sensitivity of 4×10^{-3} eV). Two-photon experimental results themselves depend on the nature of the intermediate state: while most experimental setups employ the S_1 6^1 state,[11,12,14,15] whose potential energy surface resembles that of the neutral benzene dimer, Shinohara and Nishi[16] use the S_2 state, which features a stacked geometry as in the charged dimer. Hence, their result is lower in energy, i.e., closer to the theoretical adiabatic IP value (the energy of the ion global minimum minus the energy of the neutral global minimum).

From the aforementioned experimental results, we infer that two-color experiments result in lower threshold values than their one-color counterparts, and propose a qualitative explanation as to why this is the case. Intracluster vibrational redistribution (IVR) in the intermediate S_1 6^1 state produces excess intermolecular vibrational energy, which translates into a rise of the translational and rotational temperatures of the cluster. This

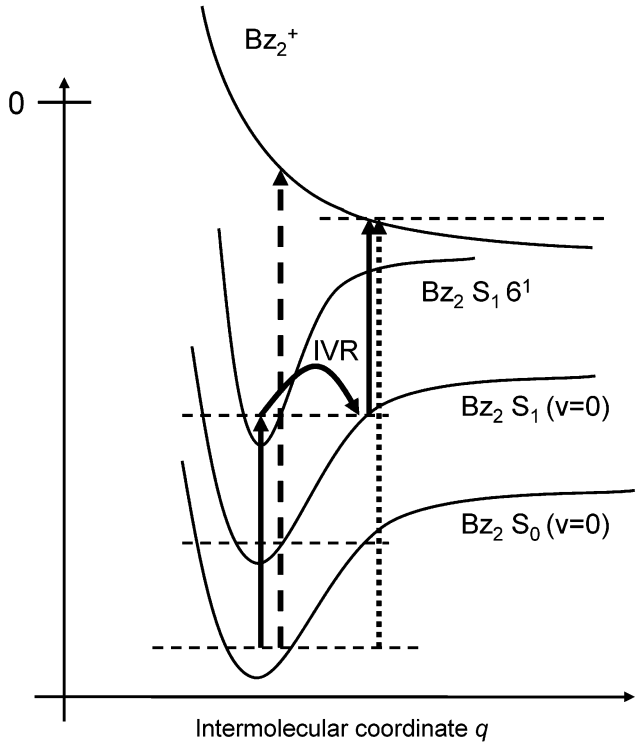

Figure 6. Schematic representation of one-photon and two-photon ionization mechanisms of the benzene dimer. One-photon ionization is denoted by the dashed arrow. Two-photon ionization (full arrows) is a multistep process: 6^1_0 transition, IVR, and ionization. The corresponding two-photon ionization potential is symbolized by the dotted arrow.

results in a broader exploration of the potential energy surface of the S_1 state (Figure 6). The IVR phenomenon produces intermediate states that feature distorted geometries and are closer to the ion structure than the corresponding neutral ground-state configuration from which they stem. The overall process, following second-photon ionization, is closer to the true adiabatic transformation and results in a lower threshold value. Assuming similarities in the respective potential energy surfaces of the S_0 and S_1 states, this phenomenon may be modeled by carrying out the molecular dynamics simulation on the neutral S_0 cluster at a higher total energy (E_0 + 300 K in our case), which, as previously mentioned, yields lower theshold values than at E_0 + 100 K. The experimental difference in energy between the 6^1 and 0^0 S_1 states being 750 K,[26] vertical ionization statistics on the configuration subspace of the $(benzene)_2$ cluster sampled by a molecular dynamics simulation at E_0 + 750 K could quantitatively confirm this picture. However, we were unable to carry out such a calculation because of frequent occurrences of monomer evaporation at this energy, which are due to the weakly bound character of the neutral benzene dimer.

IVR from the 6^1 state in the benzene dimer has been shown to be a lengthy process, with a time scale of nanoseconds or longer.[27] This does not prevent the effects of IVR from being monitored in the previously cited experiments, since a 20 ns temporal lag between excitation and ionization was employed.[11,14] In any case, the IVR process need not be complete for one to observe the aforesaid lowering of the threshold. An incomplete IVR process will result in a composite photoionization curve: the first component, due to the IVR process, is responsible for the signal at low energies, while the second component (without IVR) will only contribute at higher energies. Hence, the completeness of the IVR process does not influence

the position of the threshold but only the intensity of the signal in its vicinity.

Selectivity issues appear for larger cluster sizes, limiting the number of experimental IP determinations. Our values for $(benzene)_3$ are much higher than the ones proposed by either Krause[15] or Nishi;[16] however, the theoretically determined IP shift to lower energies when a benzene molecule is added to the dimer cluster (ca. 0.17 eV) is in better agreement with the former work (0.07 eV) than with the latter (which finds the IPs of $(benzene)_2$ and $(benzene)_3$ to be nearly equal). Krause et al. find that the IP difference between $(benzene)_3$ and $(benzene)_4$ is much smaller than that between $(benzene)_2$ and $(benzene)_3$. Our results concur, with differences of 0.01 and 0.06 eV at $E_0 + 100$ K and $E_0 + 300$ K, respectively. All values of ionization potentials are much larger than that of solid benzene, 7.58 eV.[28] As previously mentioned, larger clusters are characterized by flatter potential energy surfaces, resulting in gentler slopes on the ion current curves. This trend, already shown experimentally for clusters of benzene,[15] is confirmed by our simulations (Figure 3).

The ion intensity curve of the naphthalene dimer cluster is also characterized by a slow increase with photon energy near the threshold, which is experimentally attributed to a significant structural change between the sandwich-eclipsed (D_{2h}) structure of the transient excimer[29] and the low-energy conformation of the dimer ion.[25] As remarked by Fujiwara and Lim, the sandwich-staggered structure found to be the global minimum on the ion potential energy surface in our previous study should fit the bill, resulting in an unfavorable Franck−Condon factor. The same slow increase in the photoionization yield accompanying the rise in photon energy was also noted for higher clusters of naphthalene. We agree with Lim's explanation of a charged dimer core surrounded by additional weakly bound neutral monomers: polarization effects clearly dominate the charge resonance−polarization competition in the naphthalene trimer ion and in higher clusters.[9] The calculated values for the ionization potentials of the naphthalene clusters appearing in Table 4 are somewhat higher than those proposed by Fujiwara and Lim. However, the differences between the values tend to decrease as the cluster size grows: for $(naphthalene)_4$, the agreement between theoretical and experimental results is quite good. We note that the experimental ion current curve for $(naphthalene)_2$ rises in a markedly gentler fashion than that of $(naphthalene)_3$ or $(naphthalene)_4$,[25] as opposed to the theoretical trend explained above (section 3.3 and Figure 4). This is evidence that the Franck−Condon overlap between the intermediate excimer and the ion cluster is more unfavorable in the dimer cluster than in either the trimer or the tetramer. In the framework of our model, both the trimer and the tetramer ion feature stacked-eclipsed dimer cores of geometries similar to that of the excimer, whereas the dimer ion global minimum is a stacked-eclipsed structure, corroborating the previous assumption. Our simple ion current model, consistent with one-photon experiments only, is of course unable to reproduce these results, since the neutral clusters explored by the molecular dynamics simulation do not feature stacked geometries.

4. Conclusions

Our tailored model potential has proved its efficiency for the determination of the minimum energy structures on the potential energy surfaces of small charged and neutral aromatic clusters.[9] In this work, it is applied to the study of the photoionization mechanisms in these species. The use of classical molecular dynamics simulations ensures a more realistic description of these phenomena, by providing a better sampling of the neutral potential energy surface at total energies chosen to model the quantum effects that are thought to play an important role in the process. We hope that these results will prove to be a useful addition to a subject that is still ripe with discussion and controversy, and provide incentive for experimental studies on clusters of anthracene. Our model provides a satisfactory interpretation of experimental results in the threshold area. On the basis of available experimental data, vibrational autoionization via intermolecular modes does not seem to play an important role for the clusters under study; however, further experimental investigation in this field would surely prove constructive.

The present approach is the first step toward a dynamic modeling of ionization and charge resonance phenomena in neutral and ionic aromatic clusters. The next logical step is to adopt a mixed classical−quantum mechanical molecular dynamics procedure such as a trajectory surface hopping method. In conjunction with the valence bond Hamiltonian framework, such an approach should provide a means to carry out molecular dynamics simulations on the potential energy surfaces of the ionic clusters and their electronic excited states, thus accounting for postionization relaxation and energy redistribution within the modes of the aggregates. We are currently working to implement this methodology at reasonable CPU time costs.

References and Notes

(1) Voityuk, A. A.; Jortner, J.; Bixon, M.; Rosch, N. *J. Chem. Phys.* **2001**, *114*, 5614.
(2) Voityuk, A. A.; Siriwong, K.; Rosch, N. *Phys. Chem. Chem. Phys.* **2001**, *3*, 5421.
(3) Jortner, J.; Bixon, M.; Langenbacher, T.; Michel-Beyerle, M. E. *Proc. Natl. Acad. Sci. U.S.A.* **1998**, *95*, 12759.
(4) Hunter, C. A.; Sanders, J. K. M. *J. Am. Chem. Soc.* **1990**, *112*, 5525.
(5) Smith, G. D.; Jaffe, R. L. *J. Phys. Chem.* **1996**, *100*, 9624.
(6) White, R. P.; Niesse, J. A.; Mayne, H. R. *J. Chem. Phys.* **1998**, *108*, 2208.
(7) Spirko, V.; Engvist, O.; Soldan, P.; Selzle, H. L.; Schlag, E. W.; Hobza, P. *J. Chem. Phys.* **1999**, *111*, 572.
(8) Dang, L. X. *J. Chem. Phys.* **2000**, *113*, 266.
(9) Bouvier, B.; Brenner, V.; Millié, P.; Soudan, J. M. *J. Phys. Chem. A* **2002**, *106*, 10326.
(10) Hobza, P.; Selzle, H. L.; Schlag, E. W. *J. Phys. Chem.* **1996**, *100*, 18790.
(11) Börnsen, K. O.; Selze, H. L.; Schlag, E. W. *J. Phys. Chem.* **1988**, *92*, 5482.
(12) Ernstberger, B.; Krause, H.; Kiermeier, A.; Neusser, H. J. *J. Chem. Phys.* **1990**, *92*, 5285.
(13) Grover, J. R.; Walters, E. A.; Hui, E. T. *J. Phys. Chem.* **1987**, *91*, 3233.
(14) Selze, H. L.; Neusser, H. J.; Ernstberger, B.; Krause, H.; Schlag, E. W. *J. Phys. Chem.* **1989**, *93*, 7535.
(15) Krause, H.; Ernstberger, B.; Neusser, H. J. *Chem. Phys. Lett.* **1991**, *184*, 411.
(16) Shinohara, H.; Nishi, N. *J. Chem. Phys.* **1989**, *91*, 6743.
(17) Rühl, E.; Bisling, P. G. F.; Brutschy, B.; Baumgärtel, H. *Chem. Phys. Lett.* **1986**, *126*, 232.
(18) Grover, J. R.; Walters, E. A.; Baumgärtel, H. *J. Phys. Chem.* **1989**, *93*, 7534.
(19) Lindner, R.; MullerDethlefs, K.; Wedum, E.; Haber, K.; Grant, E. R. *Science* **1996**, *271*, 1698.
(20) Courty, A.; Mons, M.; Dimicoli, N.; Piuzzi, F.; Gaigeot, M. P.; Brenner, V.; de Pujo, P.; Millié, P. *J. Phys. Chem. A* **1998**, *102*, 6590.
(21) Gregory, J. K.; Clary, D. C. *Mol. Phys.* **1996**, *88*, 33.
(22) Hobza, P.; Selze, H. L.; Schlag, E. W. *Collect. Czech. Chem. Commun.* **1992**, *57*, 1186.
(23) Svanberg, M. *Mol. Phys.* **1997**, *92*, 1085.
(24) Wiesenfeld, J. M.; Greene, B. I. *Phys. Rev. Lett.* **1983**, *51*, 1745.
(25) Fujiwara, T.; Lim, E. C. *J. Phys. Chem. A* **2003**, *107*, 4381.
(26) Stephenson, T. A.; Radloff, P. L.; Rice, S. A. *J. Chem. Phys.* **1984**, *81*, 1060.
(27) Henson, B. F.; Hartland, G. V.; Venturo, V. A.; Felker, P. M. *J. Chem. Phys.* **1989**, *91*, 2751.
(28) Asaf, U.; Steinberger, T. *Chem. Phys. Lett.* **1975**, *33*, 563.
(29) Sadygov, R. G.; Lim, E. C. *Chem. Phys. Lett.* **1994**, *225*, 441.